Astronomy & Astrophysics manuscript no. santos_print
April 25, 2014
©ESO 2014

arXiv:1404.6135v1 [astro-ph.EP] 24 Apr 2014

The HARPS search for southern extra-solar planets.⋆

XXXV. The interesting case of HD41248: stellar activity, no planets?

N.C. Santos[1,2], A. Mortier[1], J. P. Faria[1,2], X. Dumusque[3,4], V. Zh. Adibekyan[1], E. Delgado-Mena[1], P. Figueira[1], L. Benamati[1,2], I. Boisse[8], D. Cunha[1,2], J. Gomes da Silva[1,2], G. Lo Curto[5], C. Lovis[3], J. H. C. Martins[1,2], M. Mayor[3], C. Melo[5], M. Oshagh[1,2], F. Pepe[3], D. Queloz[3,9], A. Santerne[1], D. Ségransan[3], A. Sozzetti[7], S. G. Sousa[1,2,6], and S. Udry[3]

[1] Centro de Astrofísica, Universidade do Porto, Rua das Estrelas, 4150-762 Porto, Portugal
[2] Departamento de Física e Astronomia, Faculdade de Ciências, Universidade do Porto, Rua do Campo Alegre, 4169-007 Porto, Portugal
[3] Observatoire de Genève, Université de Genève, 51 ch. des Maillettes, CH-1290 Sauverny, Switzerland
[4] Harvard-Smithsonian Center for Astrophysics, 60 Garden Street, Cambridge, Massachusetts 02138, USA
[5] European Southern Observatory, Casilla 19001, Santiago, Chile
[6] Instituto de Astrofísica de Canarias, E-38200 La Laguna, Tenerife, Spain
[7] INAF - Osservatorio Astrofisico di Torino, Via Osservatorio 20, I-10025 Pino Torinese, Italy
[8] Aix Marseille Université, CNRS, LAM (Laboratoire d'Astrophysique de Marseille) UMR 7326, 13388, Marseille, France
[9] Institute of Astronomy, University of Cambridge, Madingley Road, Cambridge, CB3 0HA, UK

Received XXX; accepted XXX

ABSTRACT

Context. The search for planets orbiting metal-poor stars is of uttermost importance for our understanding of the planet formation models. However, no dedicated searches have been conducted so far for very low mass planets orbiting such objects. Only a few cases of low mass planets orbiting metal-poor stars are thus known. Amongst these, HD 41248 is a metal-poor, solar-type star on which a resonant pair of super-Earth like planets has been announced. This detection was based on 62 radial velocity measurements obtained with the HARPS spectrograph (public data).
Aims. In the present paper we present a new planet search program that is using the HARPS spectrograph to search for Neptunes and Super-Earths orbiting a sample of metal-poor FGK dwarfs. We then present a detailed analysis of an additional 162 radial velocity measurements of HD 41248, obtained within this program, with the goal of confirming the existence of the proposed planetary system.
Methods. We analyzed the precise radial velocities, obtained with the HARPS spectrograph, together with several stellar activity diagnostics and line profile indicators.
Results. A careful analysis shows no evidence for the planetary system previously announced. One of the signals, with a period of ∼25 days, is shown to be related to the rotational period of the star, and is clearly seen in some of the activity proxies. The remaining signal (P∼18 days) could not be convincingly retrieved in the new data set.
Conclusions. We discuss possible causes for the complex (evolving) signals observed in the data of HD 41248, proposing that they may be explained by the appearance and disappearance of active regions on the surface of a star with strong differential rotation, or by a combination of the sparse data sampling and active region evolution.

Key words. planetary systems – Stars: solar-type – Stars: activity – Stars: abundances – Stars: Individual: HD 41248 – Surveys

1. Introduction

Precise spectroscopic studies of stars with giant planets show that their frequency is a strong function of the stellar metallicity. It is easier to find such a planet around a metal-rich star than around a metal-poor object (Gonzalez 1998; Santos et al. 2001, 2004b; Reid 2002; Fischer & Valenti 2005; Sousa et al. 2011b). Several studies on solar neighborhood stars have shown that at least 25% of stars with [Fe/H] above +0.3 dex (twice the solar value) have an orbiting giant planet. This frequency decreases to about 5% for solar metallicity stars. This observational result is usually interpreted as due to a higher probability of forming a giant planet core before the dissipation of the proto-planetary disk in a metal rich environment (e.g. Mordasini et al. 2009).

A number of questions are still open, however, whose answer may have strong implications for planet formation models, especially in the metal-poor regime. In the context of one of the HARPS surveys, a search for giant planets around a sample of ∼100 metal-poor stars was conducted. Three new giant planet candidates were discovered, and a fourth interesting candidate was announced (Santos et al. 2007, 2011). As expected, the results seem to confirm that metal-poor stars have a lower frequency of short-period giants (see also Sozzetti et al. 2009), and when these are found, they tend to have longer period orbits (Adibekyan et al. 2013). Curiously, however, the results also suggest that the frequency of giant planets orbiting metal-poor stars may be higher than previously thought, at least for values of [Fe/H]> −0.7 (Mortier et al. 2012).

⋆ Based on observations collected at ESO facilities under programs 082.C-0212, 085.C-0063, 086.C-0284, and 190.C-0027 (with the HARPS spectrograph at the ESO 3.6-m telescope, La Silla-Paranal Observatory).

Present numbers also indicate that the frequency of giant planets as a function of stellar metallicity may not be described by a simple power-law (as previously suggested for the metal-rich regime – Johnson et al. 2010), and may be flat for metallicities below −0.1 dex (e.g. Udry & Santos 2007; Mortier et al. 2013). A tentative lower limit of the stellar metallicity (∼−0.7 dex) below which no giant planets can be formed was also found (e.g. Mortier et al. 2013). In brief, the giant planet formation efficiency in the metal-poor regime is still a matter of lively debate. Since the metallicity is one of the most important ingredients controlling planet formation (Ida & Lin 2004; Mordasini et al. 2009), the answer to these issues is mandatory if we want to fully access the process of planet formation and evolution.

Additional information about the frequency of other types of planets (Neptune and super-Earth like) as a function of stellar metallicity is key in this discussion. In fact, contrarily to what one might expect, the known correlation between the presence of planets and the stellar metallicity that exists for stars hosting giant planets does not seem to exist for stars hosting their lower mass planetary counterparts (Udry et al. 2006; Sousa et al. 2008). Recent results have shown that stars with Neptune-mass planets have a rather flat metallicity distribution. Moreover, considering systems with only hot Neptunes (without any other Jupiter mass analog), though the number is still small, the metallicity distribution becomes slightly metal-poor (e.g. Mayor et al. 2011; Sousa et al. 2011b; Buchhave et al. 2012).

These observational facts are supported by theoretical work (Ida & Lin 2004; Mordasini et al. 2009), showing that planets in the Neptune-mass regime should be common around stars with a wide range of metallicities, while giant planets should be more common only around metal-rich stars. This can be interpreted as due to the fact that high metallicity proto-planetary disks are able to form rocky/icy cores fast enough so that gas runaway accretion will lead to the formation of a giant planet before disk dissipation occurs. In turn, lower metallicity disks will imply longer planet formation timescales, leading to a lower fraction of giant planets: cores don't grow fast enough to accrete gas in large quantities before disk dissipation and thus remain "Neptune" or "Super-Earth" like. However, given the still relatively small number of discovered low mass planets, and the reduced number of metal-poor stars surveyed (no specific survey for low mass planets orbiting metal-poor stars has been carried out), it is still not possible to conclude on the frequency of low mass planets as a function of stellar metallicity.

In this paper we present a new project that makes use of precise HARPS radial velocities to search for Neptunes and Super-Earth planets orbiting a sample of metal-poor stars. The goals of the program and the sample are presented. We then turn our attention to the case of HD 41248, a metal-poor G dwarf from our sample that was recently announced to have a pair of resonant Super-Earths or Neptunes (Jenkins et al. 2013). Using the set with more than 200 precise radial velocities measurements together with different stellar activity diagnostics, we explore the existence of the planets announced by Jenkins et al. (2013). The results of this analysis are presented and discussed.

2. The metal-poor survey

To our knowledge, no specific radial velocity survey for Neptunes and Super-Earths orbiting a sample of low metallicity stars has been carried out. To tackle this issue, we started in October 2008 a dedicated program using the HARPS spectrograph at the 3.6-m ESO telescope (La Silla Paranal-Observatory, Chile). The first set of observations, done in 3 different ESO periods between October 2008 and March 2011 (ESO programs 082.C-0212, 085.C-0063, and 086.C-0284) revealed several interesting candidates (see next section for the case presented here). However, despite the total granted 60 observing nights, the sparse time sampling of the observations did not allow us to conclude on the nature of any of the observed signals.

In order to address this problem, this initial observing program was granted an extra 80 nights over 3 years (starting in October 2012) within an ESO Large Program (190.C-0027). The goals of this program are twofold: first, to complete the search already started, and secondly to confirm the very good candidates discovered in the previous runs. Once this program is finished, we expect to be able to derive the frequency of Neptunes and Super-Earths in the metal-poor regime and compare it with the published results for solar metallicity stars and with the model predictions (e.g. Mayor et al. 2011). To achieve this goal, the idea is to obtain a number of points per star that is similar to the one obtained in the HARPS GTO survey for very low mass planets around solar neighborhood stars (e.g. Mayor et al. 2011), so that a similar detectability limit is reached.

The results of this survey will then allow us to compare the results and frequencies of Neptunes and Super-Earths with those obtained in the HARPS-Guarantee Time Observations (GTO) program to search for very low mass planets orbiting a sample of solar-neighborhood stars – centered close to solar metallicity. Together, the surveys will set important constraints for the models of planet formation and evolution (e.g. Mordasini et al. 2012). Addressing this problem will help us to provide a proper estimate for the frequency of planets (including Earth-like planets) in our galaxy.

We would like to note that, as already widely known, the search for low mass planets, which induce very low amplitude signals in the radial velocities, is a difficult and time-consuming process. This is very well illustrated by the huge number of data points that was recently required to detect the Earth mass planet around α Cen B (Dumusque et al. 2012). Further to this, a number of difficulties exist when dealing with the analysis of low amplitude signals. For instance, stellar activity may induce false positive signals that can mimic the radial velocity signature of a low mass planet (e.g. Forveille et al. 2009). Furthermore, recent results from radial velocity surveys have show that many of the low mass planets are in systems, where several planets produce overlapping signals in the data, making the analysis even more complex (e.g. Lovis et al. 2011b). The ubiquity of multi-planet systems has also been demonstrated by the results of the Kepler mission (e.g. Batalha et al. 2013).

2.1. Target selection and stellar properties

The target list was chosen based on two sub-sets of the former HARPS GTO planet search program (completed in 2009). The first was a survey for giant planets orbiting metal-poor stars (Santos et al. 2007). The second was a program to search for giant planets orbiting a volume-limited sample of FGK dwarfs (Naef et al. 2007). Both sets of stars were surveyed with a precision of ∼2-3 m s^{-1}, clearly insufficient to allow for the detection of Neptune-like planets (the observing strategy and frequency of measurements was also not adequate for this goal).

Merging these two HARPS samples, we took all stars that met the following criteria:

– Not known to harbor low mass planets;

Table 1. . List of stars in the sample, their V magnitudes, and coordinates (2000.0 equinox).

Star	V	RA(J2000)	Dec(J2000)
HD224817	8.41	00:00:58.2	−11:49:25
HD208	8.23	00:06:53.9	−03:37:34
HD967	8.36	00:14:04.5	−11:18:42
(...)	(...)	(...)	(...)

- Metallicities below −0.4 dex (derived from HARPS CCF – see e.g. Santos et al. 2002);
- Chromospherically quiet ($\log R'_{HK} < -4.8$, as measured from HARPS spectra);
- Present radial-velocity variations with a dispersion below $10\,\mathrm{m\,s^{-1}}$ (higher dispersions may imply the presence of higher mass planets);
- Brighter than V=9.5 (to allow a photon noise precision of $1\,\mathrm{m\,s^{-1}}$ after 900s).

The previous information gathered in both surveys was thus sufficient to allow for the definition of a good sample of 109 metal-deficient stars (−1.5<[Fe/H]< −0.4) that are suitable targets for the detection of very low mass planets (Neptunes or Super-Earths) – Table 1. To these we added the three long period planet host stars presented in Santos et al. (2011), whose planets were discovered in the context of the HARPS GTO program to search for giant planets orbiting metal-poor stars (HD171028, HD181720, and HD190984), as well as a fourth long period planet host candidate (HD107094). The goal is to search for very low mass planets orbiting these stars.

Stellar parameters for 106 out of the 109 targets were derived from a set of high resolution HARPS spectra taken during the HARPS-GTO program[1]. The values were presented in Sousa et al. (2011b,a). In Fig. 1 we present the distributions of [Fe/H] and effective temperature. All the stars in the sample have metallicities lower than solar, with an average [Fe/H] of −0.58. However, since these parameters were derived after the sample has been defined[2], not all stars have a metallicity below −0.4 dex: 21 stars have spectroscopic [Fe/H] values higher than this value, though lower than −0.22 dex. One single "outlier" was found to have almost solar metallicity (HD 144589, [Fe/H]=−0.05).

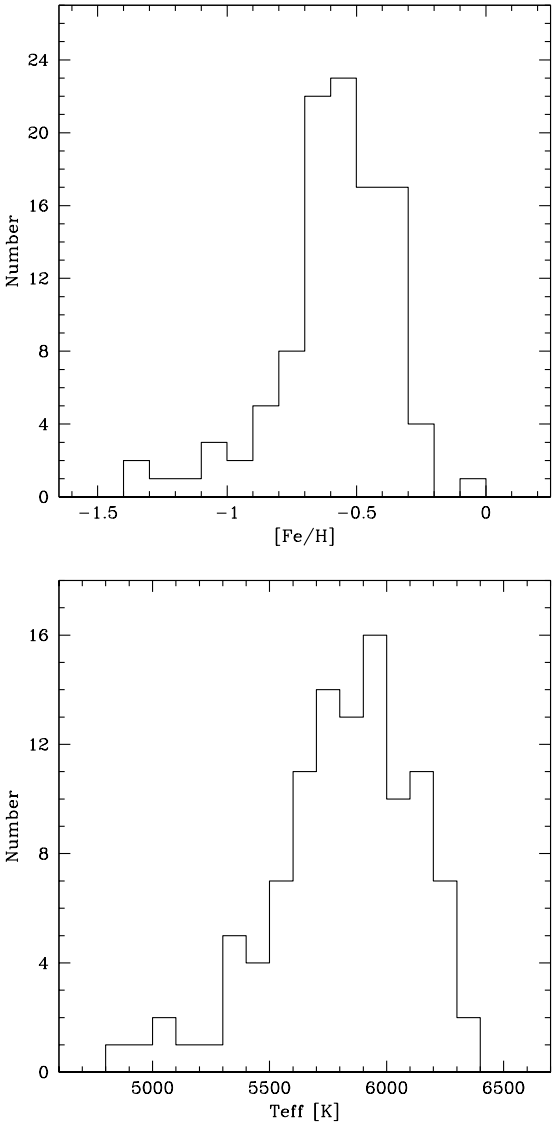

Fig. 1. Metallicity (top) and effective temperature (bottom) distributions for the stars in our sample.

3. HD41248

In a recent paper, Jenkins et al. (2013) used the first 62 (public) radial velocity measurements of the star HD 41248 to announce the detection of a system of two super-Earth or Neptune mass planets, with orbital periods of ∼18.36 and 25.65 days. While the second of these signals was not very conspicuous, the first is clear on the dataset they analyzed.

The 18-day period signal had been spotted by us in 2010. However, since its value was close to the expected rotational period of the star as computed from the activity level (see Sect. 3.1, as well Jenkins et al. 2013), and because a possible peak at the same period was also seen in the Bisector Inverse Slope (BIS) of the HARPS Cross Correlation Function (CCF) – Fig. 5 – we decided that it would be wise to gather a new batch of observations before announcing the putative planet. In the following we will present the results of the analysis of the whole date set gathered in the programs presented above.

3.1. Stellar properties

HD 41248 (HIP 28460) is a V=8.82 magnitude G2 dwarf in the southern constellation Pictor. According to the new Hipparcos catalog reduction (van Leeuwen 2007), it has a parallax of 19.22±0.79 mas, which puts it at a distance of 52±2 parsec from the Sun. Sousa et al. (2011b) derived precise stellar parameters for this star using a set of high resolution and high S/N spectra obtained during the HARPS-GTO program. The resulting values are $T_{\rm eff}$=5713±21 K, $\log g$=4.49±0.05 dex, and [Fe/H]=−0.37±0.01 dex[3]. These values are very similar to the ones listed by Jenkins et al. (2013): $T_{\rm eff}$=5713±50 K, $\log g$=4.48±0.10 dex, and [Fe/H]=−0.43±0.10 dex. Compatible values for the effective temperature are also listed in the PASTEL catalogue (Soubiran et al. 2010): Masana et al. (2006)

[1] Exceptions are HD 196877, HD 211532, and HD 304636.

[2] As mentioned above, the definition was done using values derived from a calibration of the HARPS-CCF, and not from a detailed spectroscopic analysis

[3] These errors are merely the internal uncertainties. For the surface gravity and metallicity we adopt more realistic uncertainties of 0.05 dex (reasonable given the proximity of the effective temperature to the solar one).

Table 2. Stellar parameters for HD41248.

Parameter	
Spectral type	G2V
m_v	8.82
$B-V$	0.62
Parallax [mas]	19.11±0.71
Distance [pc]	52±2
M_v	5.23
L [$L_\odot$]	0.70
$\log R'_{HK}$	−4.90
P_{Rot} [days]	20±3
$v \sin i$ [km s^{-1}]	1.0
$T_{\rm eff}$ [K]	5713±21
$\log g$	4.49±0.05
[Fe/H]	−0.37±0.05
Mass [$M_\odot$]	0.94±0.02
Radius [$R_\odot$]	0.92±0.06

derived $T_{\rm eff}$=5827 K, while Casagrande et al. (2011) obtained $T_{\rm eff}$=5927 K.

An estimate for the mass and radius of HD 41248 can be obtained using the calibration in Torres et al. (2010). The value and its uncertainty was derived using a Montecarlo approach, where random values of effective temperature, surface gravity, and metallicity as derived by Sousa et al. (2011b) were drawn taking into account the (gaussian) uncertainties. Final values of 0.94±0.02 $M_\odot$ and 0.92±0.06 $R_\odot$ were derived for the mass and radius, respectively. Using this value for the stellar mass, the effective temperature derived by Sousa et al., the parallax, the visual magnitude, and the bolometric correction of −0.09 as derived from the calibration of Flower (1996), we derive an astrometric surface gravity of 4.56 dex (see Eqn. 1 in Santos et al. 2004b), very similar to the spectroscopic value. These are typical stellar parameters for a G2, moderately metal-poor dwarf.

The analysis of the HARPS spectra (see below) also allows us to derive the stellar activity level of the star, using the Ca II H and K lines (Lovis et al. 2011a). The average value over the ∼10 years of measurements is $<\log R'_{HK}>=-4.90$, with the values ranging from −5.20 to −4.79. These values are typical for a solar-like activity star in the low activity part of the Vaughan-Preston gap (Vaughan & Preston 1980). On its side, the observed value can be used to derive an estimate for the rotational period of the star. Using the calibrations of Noyes et al. (1984) and Mamajek & Hillenbrand (2008) we obtain values for the rotational period of 19.8±3.6 and 20.1±3.0 days[4], respectively. Finally, from the FWHM of the HARPS cross correlation function we could estimate a value of 1.0 km s^{-1} for the projected rotational velocity of the star (see e.g. Santos et al. 2002), a value slightly lower than the 2.4 km s^{-1} listed by Jenkins et al. (2013).

HD 41248 is a thin-disk star both in terms of kinematics and chemistry. With a value of [α/Fe] = 0.05 dex (Adibekyan et al. 2012b), the star does not show any α-element enhancement, a characteristic that is used to distinguish thin and thick disk stars at that metallicity (Fuhrmann et al. 1998; Bensby et al. 2003; Adibekyan et al. 2012b). Its oxygen-to-iron abundance ratio, derived using the OI 6300Å line is [O/Fe] = 0.11 dex, also in agreement with the results for other α-elements. Note also that the α-enhancement has been shown to correlate with the presence of planets in the metal-poor regime (Haywood 2008; Adibekyan et al. 2012a).

[4] Uncertainties are computed from the rms of the $\log R'_{HK}$ values.

The galactic space velocity components of the star ($U_{\rm LSR}$ = -2, $V_{\rm LSR}$ = -6, and $W_{\rm LSR}$ = 34 km s^{-1}) also suggest a thin-disk origin with a probability of ∼95% (Adibekyan et al. 2012b). HD 41248 has a low Galactic orbital eccentricity (0.04) and low Z_{max}[5] of about 0.6 kpc (Casagrande et al. 2011). Finally, it shows a Li abundance of 1.56±0.10 (Delgado Mena et al. 2013). This value is typical for a star of its effective temperature, and does not reflect any particularly strong Li depletion as often found in planet-host stars of similar temperature (see e.g. Delgado Mena et al. 2013).

3.2. Radial velocities

Between October 2003 and December 2013, a total of 223 radial velocity measurements were obtained of HD 41248 using the HARPS spectrograph at the 3.6-m ESO telescope (La Silla-Paranal Observatory). The simultaneous calibration mode was used. Starting in March 2013, the simultaneous calibration was done using the available Fabry-Perot system, while before this date the ThAr lamp was used in this process. The average signal-to-noise of the HARPS spectra in order 60 (∼6200Å) is 93, with values ranging from around 20 up to 150.

An analysis of the HARPS spectra allows us to exclude problematic measurements a priori (before the radial velocity analysis). Such situation include e.g. measurements with very low S/N or spectra with an abnormal blue-to-red flux ratio. These cases are usually related with nights when the transmissions was particularly bad (e.g. the presence of cirrus) or when observations are done at high airmass values. Two of the measurements in our data set (JD=55304.518017 and 56409.495511) were excluded based on these criteria. In all the analysis presented in this paper we made use of the remaining 221 data points.

The radial velocities (RVs) were derived using the HARPS pipeline (version 3.7) making use of the weighted Cross-Correlation technique, and using a cross-correlation mask optimized for a G2 dwarf (the same spectral type as HD 41248). The average error of the RVs is 1.4 m s^{-1}. This value includes the photon noise, the calibration noise, and the uncertainty in the measurement of the instrumental drift. In all subsequent analysis, an error of 70 cm s^{-1} was further quadratically added to this uncertainty, to take into account other possible sources of noise including instrumental, atmospheric, and stellar contaminants, as well as stellar jitter (see e.g. Pepe et al. 2011). The addition of this white-noise will not introduce any inexistent signals in the data.

As presented in Sect. 2.1, the first set of RV data points obtained for this star was gathered in the context of a sub-survey of the HARPS GTO program. The goal of this sub-sample was to search for giant planets, and a corresponding strategy, in terms of precision, was adopted. As such, the error bars in a large fraction of the first dataset are significantly higher than the ones found in later measurements. Since October 2008 (when the large program started) the measurements were obtained with a completely different strategy. Exposure times were set at a minimum of 15 minutes in order to average-out the noise coming from stellar oscillations (e.g. Santos et al. 2004a). Starting in October 2012 we also decided to obtain, whenever possible, more than 1 spectrum of the star in a given night, separated by several hours. This strategy was used to minimize sources of stellar noise such as stellar oscillations and granulation and has proven to be very efficient when searching for extremely low amplitude RV signals

[5] The maximum vertical distance the stars can reach above/below the Galactic plane.

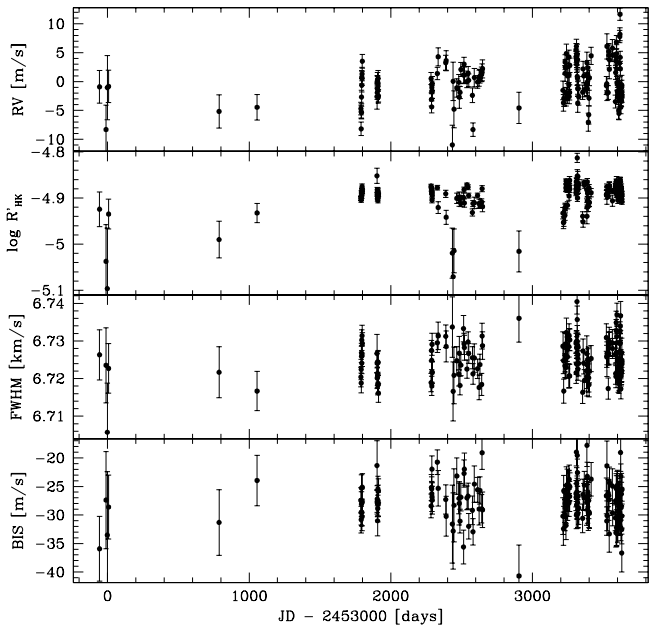

Fig. 2. Time series of the radial velocity, stellar activity, FWHM, and BIS.

(Pepe et al. 2010; Dumusque et al. 2010). Since the periodic signals we will be analyzing in this paper are much longer than one night, we used the nightly binned data in our analysis. This implies that "only" a total of 156 separate data points (in 156 different nights) are considered[6].

The HARPS pipeline also derives values for other parameters such as the Bisector Inverse Slope (BIS – Queloz et al. 2001), the Cross-Correlation Function (CCF) parameters FWHM and Contrast, as well as the activity level of the star using the Ca II K and K lines ($\log R'_{HK}$). To these, we have also separately computed (using the software described in Appendix A) a number of alternative line profile variation indicators as defined in Boisse et al. (2011, V_{span}), Nardetto et al. (2006, biGauss), and Figueira et al. (2013, V_{asy}, BIS+, and BIS−). These indices are used for the analysis and interpretation of the observed radial velocity signals.

In Fig 2 we plot the radial velocity time series, together with the derived values for the activity level and the CCF parameters FWHM and BIS. A simple look at the plots shows that the RV values show a slightly increasing trend with time. No clear trend is seen for the $\log R'_{HK}$ activity index, the FWHM, or the BIS, which suggests that this drift is not related to the variation of activity level along the magnetic cycle of the star (Santos et al. 2010; Lovis et al. 2011a; Dumusque et al. 2011).

3.3. Keplerian fitting

To test if the signals detected by Jenkins et al. (2013) are still present in the data after including the additional RVs, we decided as a first approach to use the yorbit algorithm (Ségransan et al., in prep.) to fit the whole data set with a model composed of 2 Keplerian functions and one linear trend. Yorbit uses an hybrid method based on a fast linear algorithm (Levenberg-Marquardt) and genetic operators (breeding, mutations, cross-over), and has been optimized to explore the parameter space when doing Keplerian fitting of radial velocity data sets. Since the first goal was to explore the existence of the signals announced by Jenkins et al., we chose to explore only the solutions with periods between 16 and 20 days (for the first planet), and between 24 and 28 days (for the second planet).

[6] These RV measurements are published as an electronic table

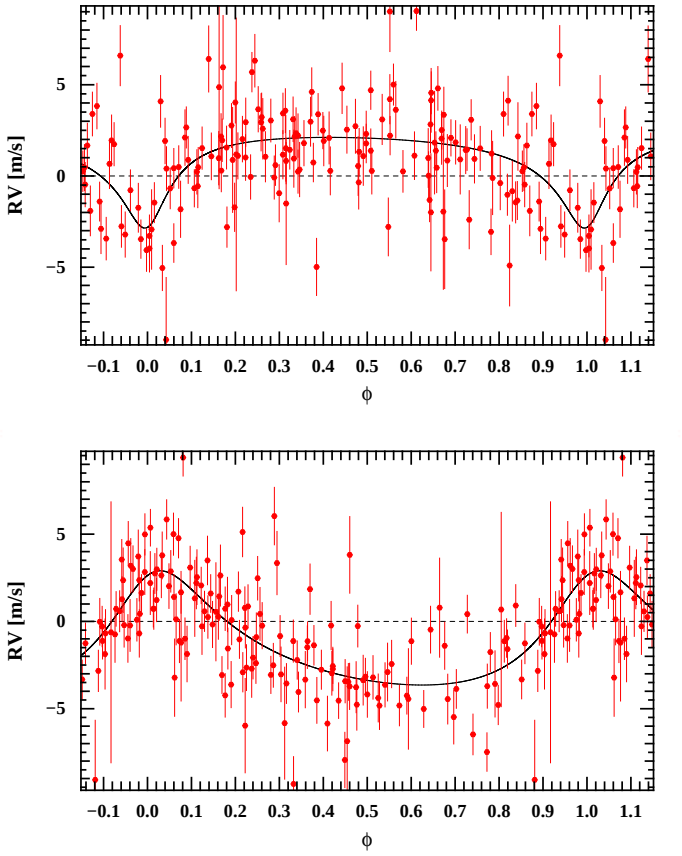

Fig. 3. Phase folded radial velocities of HD 41248 with the best fit Keplerian functions at ∼18-days (top) and ∼25 days (bottom).

The phase folded, best fit Keplerian solutions are presented in Fig. 3. The final solutions converged to orbital periods of 18.336±0.006 and 25.623±0.010 days, with eccentricities of 0.54±0.09 and 0.36±0.07 and semi-amplitudes of 2.46±0.41 and 3.32±0.26 m s^{-1}, respectively. If caused by the presence of planets, and assuming a stellar mass of 0.94 $M_\odot$, these solutions correspond to the signal induced by Super-Earth or Neptune like planets with masses of 8.2 and 13.7 $M_\oplus$, respectively. The residuals to the fit show an rms of 2.15 m s^{-1}, clearly above the average error bar of the measurements (1.4 m s^{-1}). Some structure is also present in the residuals: a Generalized Lomb Scargle periodogram (GLS, Zechmeister & Kürster 2009) shows some power at ∼30 days, though not statistically significant (the computed False Alarm Probability is around 5%). Given the complexity of the observed signals (see discussion below), in the present paper we will not discuss the nature of this signal in detail[7].

The 25-day period fit presented in Fig. 3 looks perfectly reasonable. However, the 18 day signal is visually not "convincing", as it owes its shape mostly to a few points near phase 0 (or 1). But even if it was credible, the fact that visually these solutions could be acceptable does not, of course, confirm the exis-

[7] As we will see below, a peak at this period is clearly also seen in the FWHM, BIS−, and V_{asy} periodogram of set #1 (Fig. 5).

tence of planets orbiting HD 41248. For instance, several cases have shown that stable active regions can be present in the photospheres of solar-type stars (e.g. Queloz et al. 2001; Forveille et al. 2009; Figueira et al. 2010). These may produce RV signals that mimic the ones expected from real planetary systems.

A simple comparison of the fitted signals with the ones presented in Jenkins et al. (2013) shows that the periods found are consistent. The eccentricities, however, are significantly higher than the ones (close to zero) presented by these authors. The amplitude of the 25 day period signal is also significantly above the maximum value listed by Jenkins et al. (2.97 m s^{-1}). Imposing circular orbits decreases the amplitudes to 1.99 and 2.99 m s^{-1}, respectively, but produce a slightly worse fit with an rms of 2.26 m s^{-1}. In any case, these values suggest that at least the 25-day period signal has evolved in amplitude over time.

3.3.1. Bayesian analysis with Keplerian functions

In complement, we also performed a Bayesian analysis of the whole data set following the methodology done e.g. by Gregory (2011). In this process we used large and uninformative priors, except for the orbital eccentricity for which we choose a Beta distribution as suggested by Kipping (2013). We also assumed here that the data can be modeled by a series of Keplerian orbits and a linear drift. We ran a large number of chains using the Markov Chain Monte Carlo (MCMC) algorithm implemented into the `PASTIS` software (Díaz et al. 2014). We point to this paper for more details on all the process. We then compute the Bayes factor of models with n+1 Keplerian orbits against models with n Keplerian orbits by estimating the evidence of each model using the Truncated Posterior Mixture as described by Tuomi & Jones (2012).

We found that the data can be modeled by up to five significant Keplerians with periods respectively of $P_1 = 25.628 \pm 0.011$ days, $P_2 = 18.349 \pm 0.012$ days, $P_3 = 30.715 \pm 0.031$ days, $P_4 = 12.6291 \pm 0.0034$ days, and $P_5 = 8.8^{+1.2}_{-1.7}$ days. All these Keplerian orbits are found to have significant eccentricities, except for the ones at ∼18 and ∼8.8 days. The two first Keplerian orbits are compatible with the ones reported by Jenkins et al. (2013), while P_4 and P_5 are found to be really close to $P_1/2$ and $P_1/3$.

As we will see below, we will conclude that the P_4 and P_5 are the harmonic of the stellar activity signal which has a main period $P_1 \approx 25.6$ days. We also find strong indications that the third Keplerian orbit, with $P_3 \approx 30.7$ days, is related to stellar activity.

3.4. Analyzing the periodograms

In order to take the analysis of the data one step further, we defined three different sets: set #1, which corresponds to the data that was used by Jenkins et al. (JD up to 55647), set #2 with JD between 55904.8 and 56414.5, and set #3 with JD between 56521.9 and 56632.7. Sets #2, and #3 correspond to two different observing seasons, and are separated by a temporal gap (due to the passage of the star "close" to the Sun). The number of points in each data set is 61, 50, and 45, respectively for set #1, #2, and #3. In the following, and before dividing the data in the three different sets, we fitted and subtracted from the RVs a linear trend (Fig. 4), with a slope of 0.52±0.14 m s^{-1}/yr. Since the signals we are exploring in this paper are all of relatively short period, this decision will not have an impact on the presented results.

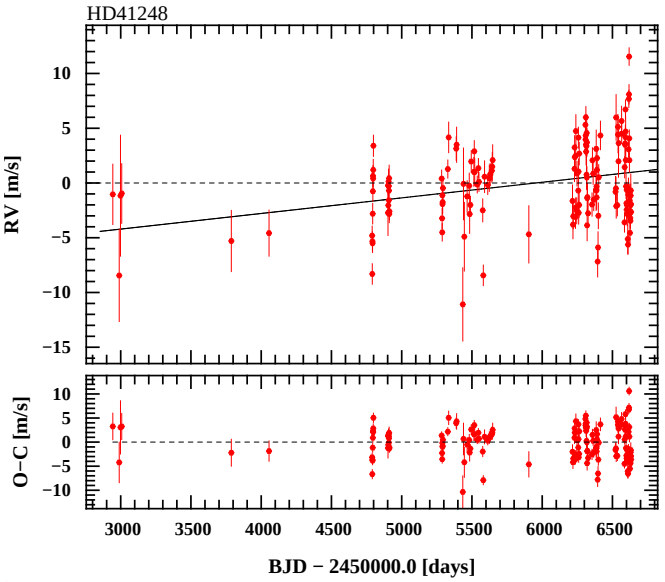

Fig. 4. Time series of the radial velocity and a linear fit to the data. The residuals are shown in the lower panel.

In Figs. 5, 6, 7, 8 we present, from top to bottom, the GLS of the RV, FWHM, BIS, $\log R'_{HK}$, BIS−, BIS+, biGauss, V_{asy}, and V_{span} for the data in sets #1, #2, #3, as well as for all our data together, respectively. In all the plots, the horizontal line denotes the 1% False Alarm Probability (that we will consider as the significance limit). This value was computed using a permutation test; more details can be found in Mortier et al. (2012). The vertical dashed lines denote the locus of the 18- and 25-day periods.

In set #1 (Fig. 5), the highest and only significant peak in RV is at ∼18 days, as already pointed out in Jenkins et al. (2013). This peak corresponds to the signal that these authors attributed to the presence of one of the planets. No similarly significant peak is seen in any of the other indices, though a clear peak near 18 days is also observed at least in the BIS and BIS+ line profile indicators. The peak at ∼25 days, which corresponds to the second candidate planet announced by Jenkins et al., also has some power in the FWHM and V_{asy}, though never at a significant level. A peak close to 25 days is also present in $\log R'_{HK}$. Finally, a peak close to 30 days (one of the periods mentioned in Sect. 3.3.1) is also seen in FWHM, BIS−, and V_{asy}.

For data set #2 alone, the periodograms, presented in Fig. 6, show that no significant peaks are detected in any of the variables. In RV, a forest of peaks is present, the most conspicuous a peak at ∼35 days (with some power also at similar value in FWHM, BIS+, and V_{asy}), followed by the one at ∼25 days. This signal, at or close to 25 days, is also seen in all the remaining variables, with exception of the V_{span}. For RV, no peak is present at 18 days, though clear peaks close to that period are observed in BIS, BIS+, biGauss, and V_{span}. Finally, a clear peak at ∼60 days is seen in all the variables analyzed, with exception of V_{asy}.

For data set #3, Fig. 7 shows that for RV, FWHM, and $\log R'_{HK}$ there is a clear signal at 25 days, as well as at its first harmonic (P/2∼12.5). No clear signal is observed at 18.36 days, though a non-significant bump in the peridogram exists at ∼19 days. A peak at ∼19 days is also seen in the periodogram of the FWHM. Interestingly, the periodogram of BIS, BIS−, BIS+, biGauss, and V_{span} shows the presence of a significant peak at

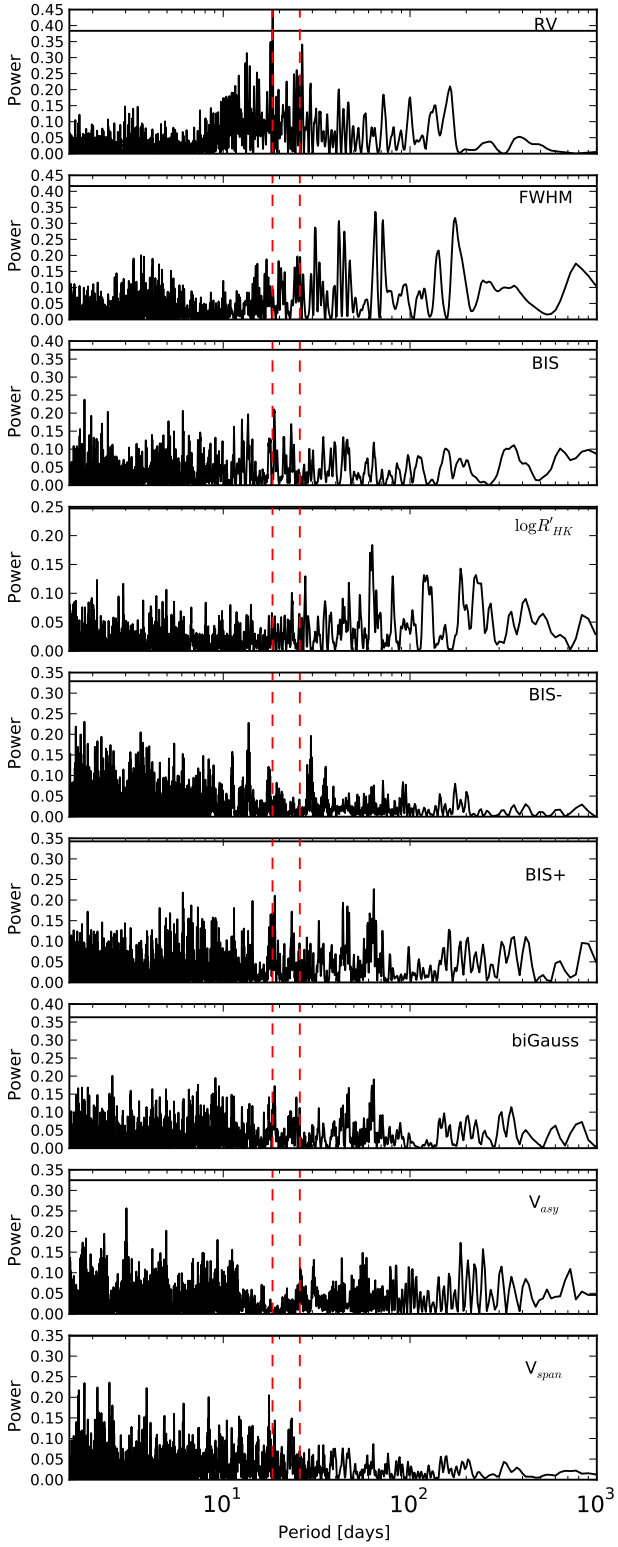

Fig. 5. Periodograms of (from top to bottom) the RV, FWHM, BIS, $\log R'_{HK}$, BIS−, BIS+, biGauss, V_{asy}, and V_{span} for data set #1. The horizontal line denotes the 1% false alarm probability level. Vertical dashed lines denote the position of the 18.36 and 25.7 day signals as found by Jenkins et al. (2013).

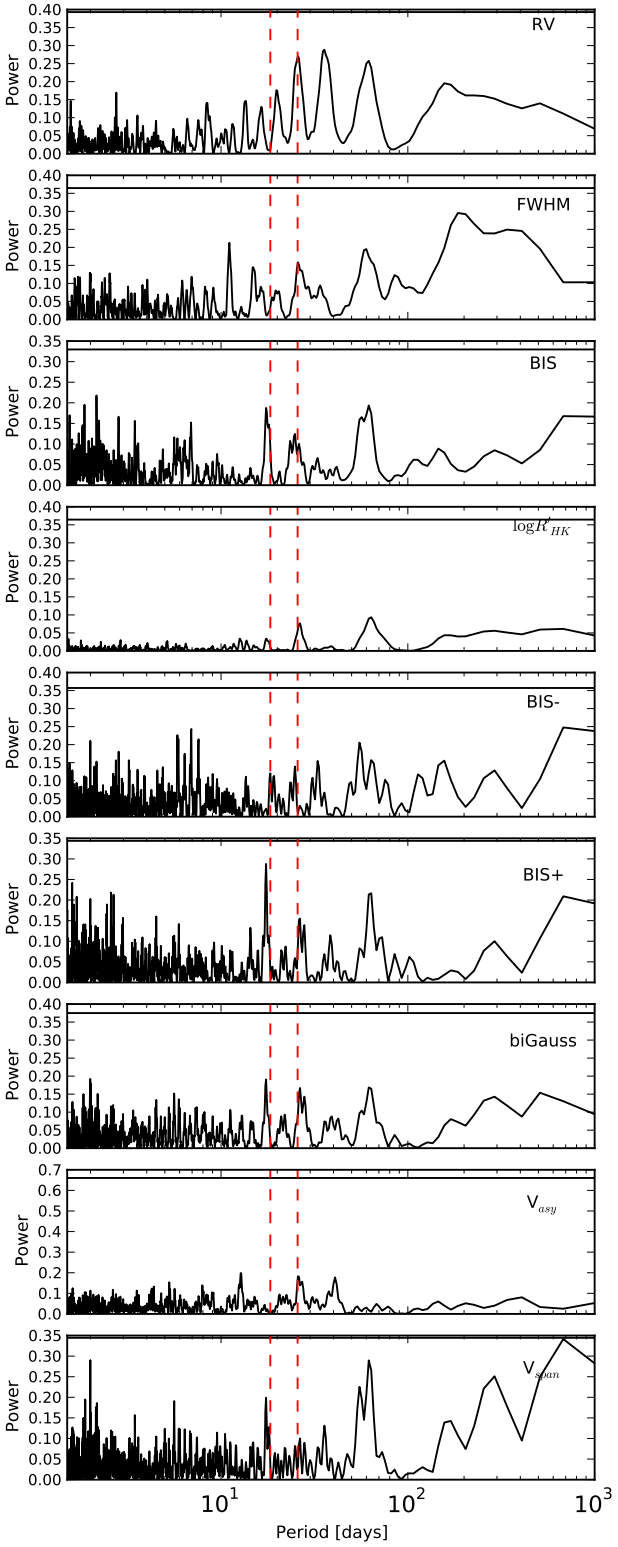

Fig. 6. Same as Fig 5 for data set #2.

~4.5 days, a value that is 1/4th of 18 days. The cause for this peak will not be discussed further as we don't have any clear explanation for its existence.

Finally, the periodograms of the whole data set (Fig. 8) show, as already mentioned above, that the pattern observed in RV is

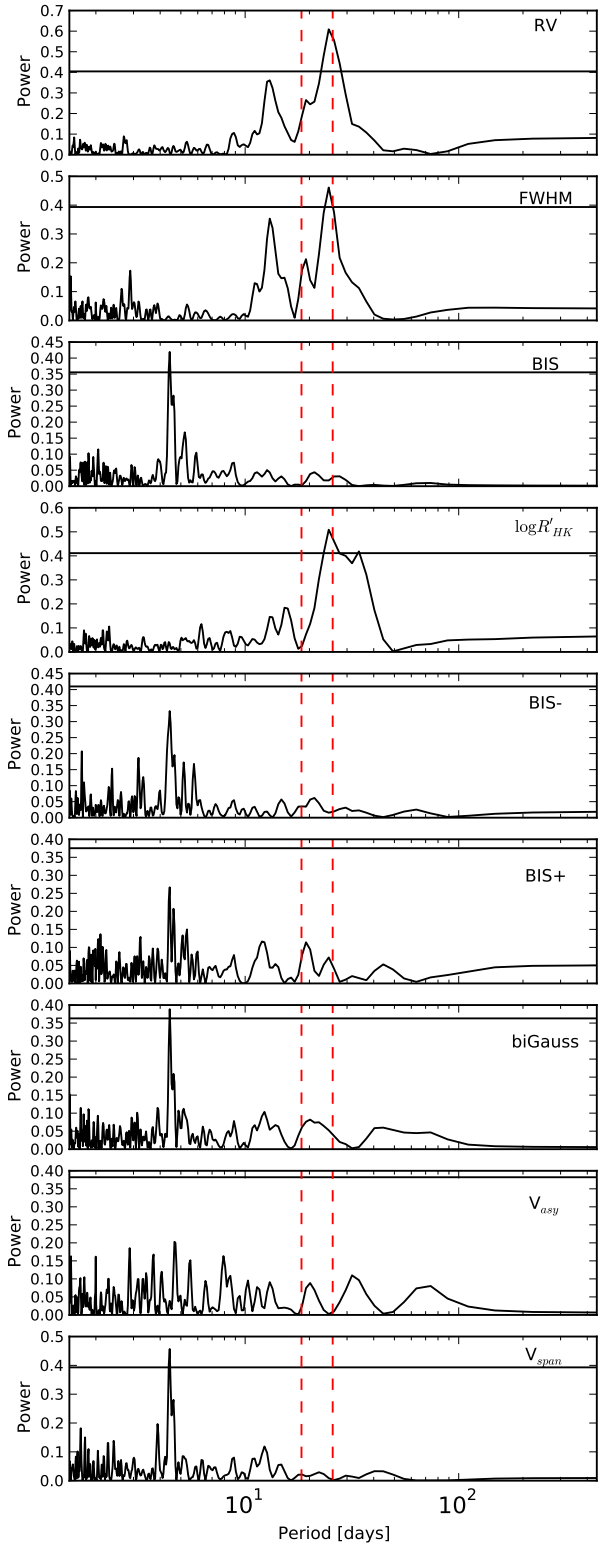

Fig. 7. Same as Fig 5 for data set #3.

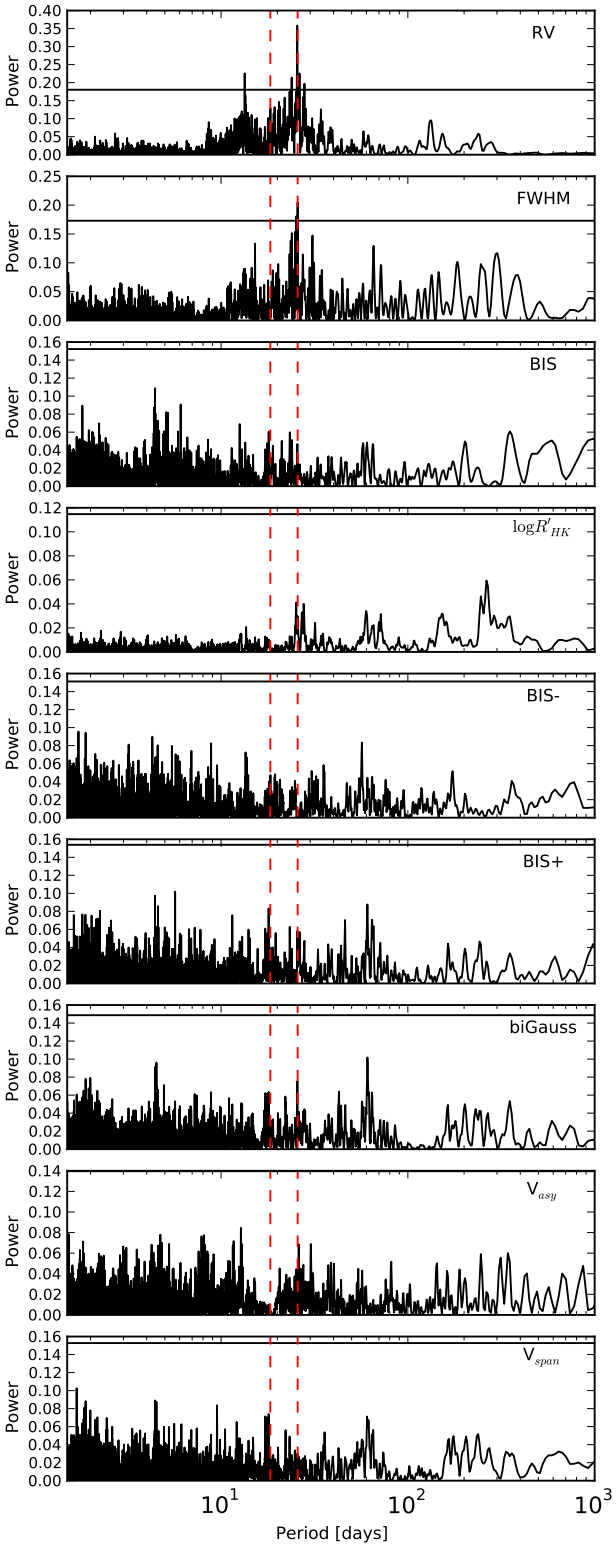

Fig. 8. Same as Fig 5 for all the data.

also well reproduced in the FWHM, with the clear and significant 25 day period signal present in both variables (the first and second harmonics, P/2 and P/3, are also visible at least in the RV). No peak at 18 days is seen in the periodograms, though a hint of power at ∼19.5 days is seen in the FWHM. The GLS of BIS, BIS+, biGauss, and V_{span} also shows some power close to 18 days, but no significant peak is seen. A peak around 31 days is also observed in the FWHM and in V_{asy}.

Noteworthy also is the fact that the amplitude of the ∼25-day period signal seems to increase as we move from set #1 to set #3.

The analysis of the RV and $\log R'_{HK}$ periodograms further shows that its phase did not significantly vary over time. In complement with the analysis presented below, this suggests that we may be in the presence of a signal produced by an evolving (growing) active longitude (Berdyugina & Usoskin 2003; Ivanov 2007), that kept its position in the stellar disk approximately constant over the last years.

In brief, the periodogram of the RV shows a complex pattern, that clearly evolves as a function of time, rendering our analysis of the data complex and difficult. The same is true for the activity and line-profile indicators. The periods found by the Bayesian fitting procedure mentioned above, for example, are all correspondent with peaks in stellar activity or line profile indicators, varying over time.

We should note that in a case where multiple signals (e.g. red noise or other Keplerians) with high enough, significant amplitudes are present in the data, one coherent signal may in principle remain undetected by a periodogram analysis, even if it is still present in the data (since it will may be diluted by the remaining signals). This problem is actually present in any analysis of data in the absence of a full model. Several of the tests presented here and in the following sections are thus valid under the assumption that no additional, sufficiently stronger signals exist that can (at least completely) hide the periodicities we are testing. Note however that all our analysis is based on several diagnostics, rendering it more solid.

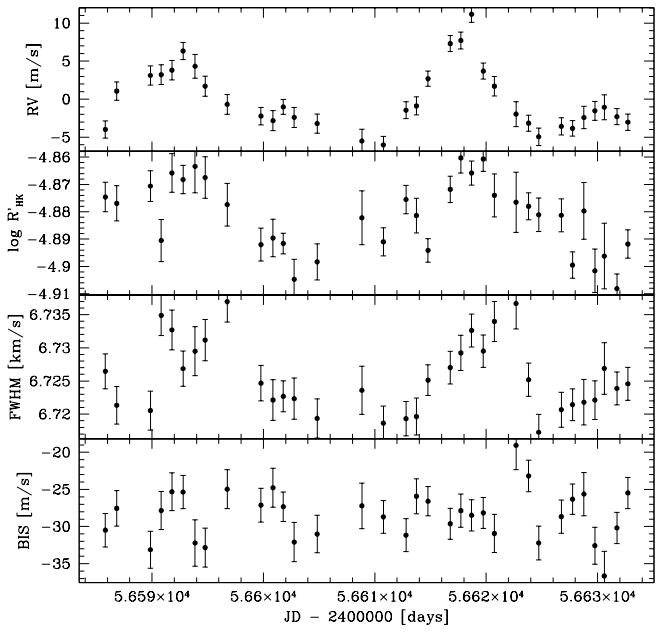

Fig. 9. Time series of the radial velocity, stellar activity, FWHM, and BIS for the period between JD= 2456580 and 2456640.

3.5. The 25-day period

As discussed in Sect. 3.4, from the analysis of the whole data set there is no sign of the 18-day period signal clearly observed in Jenkins et al. (2013). However, a distinctive peak at ∼25 days dominates the GLS. A second and third peak, at about ∼13 and ∼8.5-days are also observed. These two peaks are at the approximate position of the first and second harmonics of the ∼25-day period.

The periodogram can be interpreted in the light of at least three distinct scenarios: i) the observed signal is induced by the presence of one eccentric planet (as fitted in Sect. 3.3) with a period of 25-days (whose Keplerian signal produced a periodogram showing the periods and its harmonics), ii) we are in the presence of a system of several planets with periods that are in resonance with the 25-day period signal (see Sect. 3.3.1), or iii) we are in the presence of a signal induced by stellar spots or other activity related phenomena. The pattern observed is indeed very similar to the expected RV signal caused by a spotted star as presented and discussed in Boisse et al. (2011).

In Fig. 9 we present the time series of the RV, $\log R'_{HK}$, FWHM, and BIS for the last series of RV data, obtained in the end of 2013 (corresponding to the last measurements of set #3). As we can see from the plot, there is a clear correlation between the RV and both the FWHM and the stellar activity index $\log R'_{HK}$. With this information we conclude that the 25-day period signal observed in RV (and its harmonics) most likely corresponds to the rotational period of the star, and that the RV signal observed is caused by the rotational modulation of activity features on the stellar photosphere. The 25-day signal announced by Jenkins et al. (2013) is thus most likely better explained by stellar activity and not by the existence of a planet orbiting HD 41248.

We should note that the analysis of the GLS periodograms shows that the phase of the RV signal plotted in Fig. 9 (and in particular the peak in its value) is about ∼35 and ∼15 degrees behind the one observed in FWHM and $\log R'_{HK}$, respectively. This lag is expected if the RV signal is induced by stellar spots (see e.g. Forveille et al. 2009). Indeed, when the active regions are appearing and occupy the blueshifted side of the star, the RV will show an increasing value with time. Simulations with the SOAP code (Boisse et al. 2011)[8] show that the maximum of this RV will occur when the spots are ∼45 degrees from "meridian" (or close to disk center). Given the simple physics[9] used in the model, we consider that this number is compatible with the observed value. The value will then decrease to zero when the spot is at "meridian". This instant sets the maximum activity level as the active region shows its maximum projected area[10].

As a complementary test, we computed the Pearson's correlation coefficient (ρ) between the RV and the different line profile indicators for data set #3. For the correlation with FWHM, a value of ρ=0.52 was obtained. A Monte Carlo simulation was then done to calculate the probability of reaching this value due to a change alignment of the data points. This test was done by performing a Fisher-Yates shuffling of the values of RV and FWHM 100 000 times, computing the correlation coefficient for each simulated dataset, and deriving the distribution of the resulting ρ values. For details about the method and its background we point to Figueira et al. (2013). The test showed that the observed ρ is at 4.5 sigma from an uncorrelated (shuffled) distribution, meaning that it is very unlikely that it is caused by a chance event. Note that despite the significant correlation found, the value of ρ is not particularly high. This is due to the fact that the RV and the different line profile indicators are usually not correlated with a 1:1 relation, among other reasons (see e.g. Figueira et al. 2013). This point is also illustrated by the phase shift observed between the FWHM and RV as discussed above.

[8] http://www.astro.up.pt/soap

[9] The present SOAP version does not include, e.g., the modeling of convective blueshifts, which are different in active regions.

[10] This would also correspond to the maximum photometric variability.

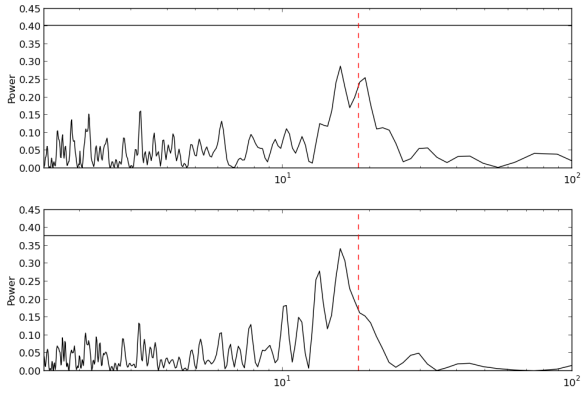

Fig. 10. Periodograms of the residuals of the harmonics fit described in Sect. 3.6.1, making use of the RV (top) and FWHM (bottom) to fix the period used to subtract the RV signal and its harmonics. The dashed line indicates the position of the 18.36 day period. The horizontal line represents the 1% FAP.

3.6. The 18-day period

The result presented above does not *per se* discard the presence of planets orbiting HD 41248 at other periods. In particular, they do not allow us to discard the existence of an 18-day period signal as present in the first batch of data and interpreted by Jenkins et al. (2013) as caused by the presence of a super-Earth mass planet.

As discussed above, however, if we divide the whole data set in three different groups, the GLS analysis suggests that 18-day period signal is only observed in the first dataset (set #1), which corresponds to the data used by Jenkins et al. No signature of the 18-day period is visible in the remaining data, even if the number of points in sets #2 and #3 are similar to the ones in set #1. One can then ask if the 18 day period signal is still present in the data, i.e., if it is constant over time, or alternatively if it was only present in the first data set. To address this issue we decided to make a series of tests, as follows.

3.6.1. Subtracting the 25-day period signal

Set #3 has, by far, the best time coverage of the data. That makes it particularly suitable to analyze the existing signals. We thus decided to analyze this set in detail to test if the 18-day period signal can be retrieved after removing the signal at 25-days.

To do this we used the approach of Boisse et al. (2011) to fit the rotational period and its harmonics, as successfully done by Dumusque et al. (2012) for the case of α Cen B. Heretofore we applied two methods. In the first one, we fitted a P∼25 day sinusoidal, together with the first harmonic (at P/2) to the RV time series. In the second case we decided to use the FWHM variation as a proxy for activity-induced RV variations, and fix P using the analysis of the FWHM signal. This procedure allows us to guarantee that in the fitting process we are not absorbing signals that are e.g. present in the RV but are not induced by activity related phenomena (e.g. real planetary signals). The residuals of the fit using both methods were analyzed.

The results of both tests can be seen in Fig. 10, where we present the GLS of the residuals to both fits. In both panels, the dashed line indicates the 18.36 day period, while the horizontal line represents the 1% FAP. As can be seen in the plots, no significant peak exist at ∼18 days. The highest peak in each plot is at 15.77 and 15.94 days, respectively. The second highest signal in the top panel is at a period of 19.02.

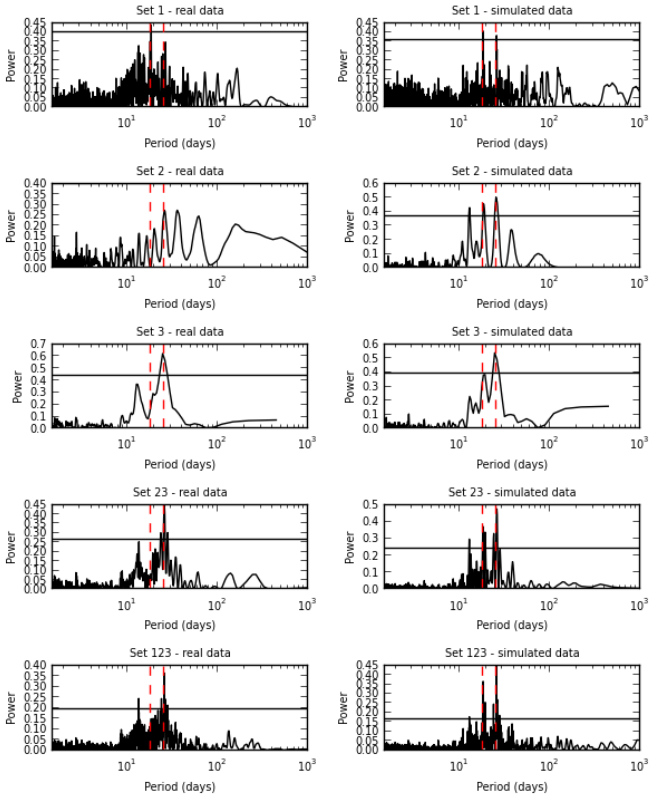
Set 1 - real data
Set 1 - simulated data
Set 2 - real data
Set 2 - simulated data
Set 3 - real data
Set 3 - simulated data
Set 23 - real data
Set 23 - simulated data
Set 123 - real data
Set 123 - simulated data
Power
Period (days)

Fig. 11. Periodograms of the different data sets, both of the real data (left) and simulated data (right). Vertical dashed lines represent the position of the 18- and 25-day signals presented in Jenkins et al.

Although not conclusive, this test does not lend support to the planetary explanation for the 18.36-day signal presented in Jenkins et al. (2013). In fact, as we will see in the next section, if that signal was present in data set #3 it should have been easily spotted. We assume here that no significantly stronger signal at other period was present that could "mask" it. The absence of any strong peak in the GLS of Fig. 10 at any other period gives support to this assumption.

3.6.2. Simulating the data

As a second test, for each of the 3 time series of data mentioned above, we generated a set of full synthetic radial velocities. The data was generated considering the real observed dates to mimic the real time sampling. The error bars for each RV point were also kept as in the original data. On each data set, we first added a Keplerian signal of ∼18.36-day period as observed by Jenkins et al. (2013). White noise was then added to each point in agreement with the error bars to simulate the different average measurement errors in each data set.

On top of this we injected a signal of 25-days into the data, as fit to the last data set where the time coverage of the data clearly allows us to model the 25-day signal. Again, the fit was done using the approach in Boisse et al. (2011), i.e., fitting the rotational period and its first harmonic (P/2)[11]. On each of the 3 datasets (set #1, #2, and #3), however, the injected 25-day period

[11] The third harmonic, or P/3, did not present a significant power.

signal was varied in amplitude until the rms of the synthetic data is the same as measured in the real data.

Note again that we find evidence that the observed activity signature has been growing over time. Not only do the periodograms show that the 25-day peak increases its significance from set #1 to set #3, but the rms of the data also increased from 2.6 m s^{-1} in set #1 to 3.0 m s^{-1} in set #2, and finally to 3.2 m s^{-1} in set #3.

In Fig. 11 we present both the observed and simulated periodograms of the data for the whole data set (set #123), as well as for set #1, set #2, set #3, and for sets #2 and #3 together (set #23). As we can see from the plots, while in the simulated data the 18-day period signal was always clear (even if often with an amplitude lower than the one seen for the 25-day period signal), the situation in the real data is different: except for the first set of data (set #1), the 18-day period signal is not observed in any other data set. In other words, the simulations presented here suggest that the signal at 18 days should in principle have been clearly detected in sets #2 and #3 if it had the same amplitude and phase as found in set #1. Once again this result does not support the scenario of the existence of an 18-day period signal as reported in Jenkins et al. (2013).

3.6.3. Bayesian analysis including activity

To further test if the 18-d signal is supported by the new data, we performed a new Bayesian analysis following the same procedure as in Sect. 3.3.1 but using data set #3 alone. This time, however, we modeled the 25-day period activity signal as in Sect. 3.6.1, using two sines at P_{rot} and $P_{rot}/2$ (Boisse et al. 2011).

We then computed the Bayes factor between the following two models: an activity signal at ∼25d with a Keplerian at ∼18 days and a ∼25d activity signal alone. The results indicate that, statistically, we cannot distinguish between the two models. This therefore strongly suggests that the 18-d planet, as found by Jenkins et al. (2013), is not confirmed (though also not rejected) by the new observations of dataset #3.

4. Analyzing the residuals: planet detection limits

Assuming that the 18- and 25-day signals detected in set #1 are purely of stellar origin (induced by activity), we can test if any other signal exists in the data that can be attributed to a planet.

As a first note of caution, its important to note that at present we do not have the necessary tools to model the whole dataset in a correct, physical way. This is because the activity pattern in HD 41248 has been shown to be complex, inducing clear but variable signals in amplitude and (likely) in period as a function of time. No strictly periodic signal is thus valid when modeling the whole data, independently of the methodology used for the fit (e.g. frequentist analysis vs. bayesian fittings). This implies that we cannot simply model the whole data set with e.g. a series of Keplerian functions.

To test the existence of further signals, we then first removed the two signals present in the first data set by fitting a 2-Keplerian function. The best fit found is similar to the one derived by Jenkins et al. (2013), though in our case we found an eccentricity of 0.38 for the 18-day period Keplerian fit. Note that the 25 day period signal is not statistically significant in data set #1. However, since it has been shown to be coherent and have the same origin as the clear signal found in set #3, we decided to remove it.

For set #2, since no significant peaks appear in the RV periodogram, we have not removed any signal. For set #3 we again removed the 25-day signal and its first harmonic as discussed in Sect. 3.6.1, while fixing P using the RV dataset itself.

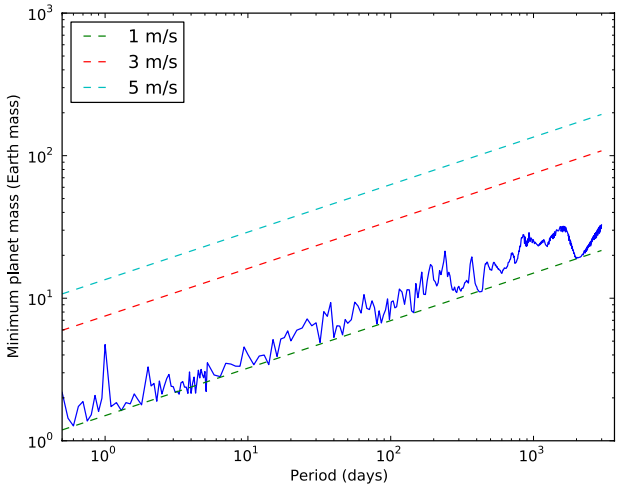

Fig. 12. Minimum planetary mass against period. The solid line represents the detection limits. The dashed lines indicates a circular planetary signal with RV semi-amplitude of 1, 3 and 5 m s^{-1}.

After removing the different signals in the 3 different sets we analyzed the joint data using the GLS. The results show that the highest peak appears at 193 days, but a permutation test shows that it is not significant (it has a False Alarm Probability of 30%).

With this set of residuals we could also derive the detection limits of potential planets present in the data. For this we used the same approach as in Mortier et al. (2012). The results of this analysis are presented in Fig. 12, and suggest that we can reasonably exclude any planets with mass above 10 $M_\oplus$ in the period range up to ∼100 days. This value decreases to ∼4$M_\oplus$ if we restrict the period range to below 10 days.

Note that the results do not significantly vary when you use the FWHM to fix P when removing the signal in set #3. Also, no significant differences are observed if we only subtract the 18-day period signal in set #1.

5. Discussion and conclusions

In a recent paper, Jenkins et al. (2013) reported the existence of a system of two low-mass planets orbiting HD 41248 in almost circular orbits of periods ∼18 and 25 days. In this paper we analyzed this system after adding almost 160 new radial velocity points obtained with the HARPS spectrograph.

The results of this analysis do not allow us to confirm the planetary origin of the signals observed in the RV data of HD 41248 as previously suggested by Jenkins et al. (2013). The observed 25-day period signal is almost exactly reproduced in the stellar activity index $\log R'_{HK}$ as well as in the FWHM of the HARPS CCF. This signal has a complex structure and varying amplitude with time, making it difficult to model with present day tools. This fact renders the analysis of the putative 18-day periodicity difficult. However, although we cannot fully discard the existence of a stable, periodic signal at 18 days as expected from the presence of a planet, the different tests that we conducted show that the current data (both the RV and activity/line profile indicators) does not support its existence. In brief, the 25-day period signal detected by Jenkins et al. (2013) is best explained as induced by stellar activity phenomena. Our analysis also suggests that the 18-day signal may have a similar origin.

We assume here that at a period of 25-days, a Neptune like planet will not be able to induce strong tidal or magnetic interactions with the star, which could result in an activity signature with a period similar to the orbital period of the planet (Saar & Cuntz 2001; Shkolnik et al. 2003)[12]. We note that cases have been found where the orbital period seems to coincide, within the uncertainties, with the rotational period of the host star (Santos et al. 2003). If this is the case for HD 41248, the low amplitude of the signals and the complexity of the data will make it very difficult to confirm.

The complexity of the signals observed and the estimate for the rotational period of the star (∼20 days – Table 2) leads us to propose that the observed 18 day and 25 day signals may be caused by at least two different active regions/longitudes in a star presenting a strong differential rotation pattern. In this scenario, the 18 and 25 day period signals would imply a differential rotation with an amplitude of about 25%. The Sun itself rotates, at the equator, with a rotational period of 26 days, while at the poles the value increases to ∼35 days. Higher levels of differential rotation have been found in earlier type stars (Barnes et al. 2005; Reiners 2006; Ammler-von Eiff & Reiners 2012; Reinhold et al. 2013)[13]. A difference in rotational period of 25% in the surface of HD 41248 seems thus perfectly plausible. This scenario would explain the existence of a growing 25-day period signal, caused by a growing active region that kept its phase all over the period of our measurements, as well as the disappearance of the 18-day period signal, if caused by an active region that disappeared (or became much weaker) and was positioned at a lower stellar latitude. It would also provide a simple explanation for the forest of peaks observed in data set #2, if we assume that other active regions may have appeared and disappeared at other latitudes.

One alternative scenario to explain the observed complex pattern is related with the fact that the data presented above present a very complex structure. It is clear from the plots that the activity patterns we are observing in this star present signatures of having evolved over the timespan (more than 10 years) of our measurements. An interesting hint may come, however, from the study of Lanza et al. (2003) where the authors analyzed the rotational period of the sun using the Total Solar Irradiance (TSI) observed during the maximum of the eleven-year cycle. In the Sun, large spot groups have typical lifetimes of 10-15 days, while the rotational period is close to 25 days. The fact that the timescales for spot evolution are shorter than the rotational period, together with the appearance and disappearance of new spot groups in different rotational phases, renders the derivation of rotational periods (from the data) a complex issue. As a result, Lanza et al. (2003) have found that, during the 1999-2001 period when the Sun was close to solar maximum, it was impossible to properly retrieve the rotational period of the Sun using the TSI data, as the analysis yielded values from 24 up to 31 days. Given the complex pattern of data presented in the present paper for HD 41248, together with the uneven sampling, the presence of signals at 18 and 25 days may simply reflect a difficulty in fitting the data properly (at least using "simple" Keplerian functions).

The present paper presents a good example of how difficult the analysis of radial velocity data can be when searching for very low-mass planets that induce low-amplitude signals, close to the measurement precision. The results also point very clearly the importance of following a star for a sufficiently long period of time until one can confidently secure the characterization of the whole system, including the effects of stellar activity. In this particular case, a proper sampling of the data (as in set #3) was fundamental to disentangle the sources of the radial velocity signals.

This study also shows that Bayesian analysis are not immune from false-positive detections, especially in the presence of stellar activity which might not be approximated by a series of Keplerian functions. The present case also demonstrates how important it is to make use of methodologies and tools to model and understand the signals produced by stellar activity. A complete characterization of the data may imply the development of more detailed physical models of stellar activity and its impact on radial velocity measurements (e.g. Boisse et al. 2012), as well as of more sensitive diagnostic methods (e.g. Figueira et al. 2013). Without that it will be very difficult to fully analyze these systems with any statistical/fitting procedure. The amplitudes of the RV signals imposed by stellar activity are, even in the case of a relatively inactive star such as HD 41248, often of the same order of magnitude as the expected signals due to a low mass planet. Alternatively, complementary spectroscopic measurements using other wavelengths (e.g. near-IR) may be useful to disentangle real planets from activity induced signals (e.g. Huélamo et al. 2008; Prato et al. 2008; Figueira et al. 2010). A new generation of near-IR spectrographs is presently being developed (e.g. CARMENES and Spirou – Quirrenbach et al. 2014; Delfosse et al. 2013), opening great perspectives in this domain.

Acknowledgements. We would like to thank N. Lanza for the fruitful discussions. We acknowledge support from Fundação para a Ciência e a Tecnologia (FCT, Portugal) through FEDER funds in program COMPETE, as well as through national funds, in the form of grants reference PTDC/CTE-AST/120251/2010 (COMPETE reference FCOMP-01-0124-FEDER-019884), RECI/FIS-AST/0176/2012 (FCOMP-01-0124-FEDER-027493), and RECI/FIS-AST/0163/2012 (FCOMP-01-0124-FEDER-027492). This work was supported by the European Research Council/European Community under the FP7 through Starting Grant agreement number 239953. NCS and PF were supported by FCT through the Investigador FCT contract references IF/00169/2012 and IF/01037/2013 and POPH/FSE (EC) by FEDER funding through the program "Programa Operacional de Factores de Competitividade - COMPETE. X. Dumusque was supported by the Swiss National Science Foundation. This work made use of the SIMBAD database.

[12] Or possibly half the orbital period in case of tidal interaction.

[13] Gastine et al. (2014) suggest that the cooler stars may even present antisolar differential rotation, where the poles rotate faster than the equator.

References

Adibekyan, V. Z., Delgado Mena, E., Sousa, S. G., et al. 2012a, A&A, 547, A36
Adibekyan, V. Z., Figueira, P., Santos, N. C., et al. 2013, A&A, 560, A51
Adibekyan, V. Z., Sousa, S. G., Santos, N. C., et al. 2012b, A&A, 545, A32
Ammler-von Eiff, M. & Reiners, A. 2012, A&A, 542, A116
Barnes, J. R., Collier Cameron, A., Donati, J.-F., et al. 2005, MNRAS, 357, L1
Batalha, N. M., Rowe, J. F., Bryson, S. T., et al. 2013, ApJS, 204, 24
Bensby, T., Feltzing, S., & Lundström, I. 2003, A&A, 410, 527
Berdyugina, S. V. & Usoskin, I. G. 2003, A&A, 405, 1121
Boisse, I., Bouchy, F., Hébrard, G., et al. 2011, A&A, 528, A4
Boisse, I., Pepe, F., Perrier, C., et al. 2012, A&A, 545, A55
Buchhave, L. A., Latham, D. W., Johansen, A., et al. 2012, Nature, 486, 375
Casagrande, L., Schönrich, R., Asplund, M., et al. 2011, A&A, 530, A138
Delfosse, X., Donati, J.-F., Kouach, D., et al. 2013, in SF2A-2013: Proceedings of the Annual meeting of the French Society of Astronomy and Astrophysics, ed. L. Cambresy, F. Martins, E. Nuss, & A. Palacios, 497–508
Delgado Mena, E., Israelian, G., González Hernández, J. I., et al. 2013, ArXiv e-prints
Díaz, R. F., Almenara, J. M., Santerne, A., et al. 2014, ArXiv e-prints
Dumusque, X., Lovis, C., Ségransan, D., et al. 2011, A&A, 535, A55
Dumusque, X., Pepe, F., Lovis, C., et al. 2012, Nature, 491, 207
Dumusque, X., Udry, S., Lovis, C., Santos, N., & Monteiro, M. 2010, A&A
Figueira, P., Marmier, M., Bonfils, X., et al. 2010, A&A, 513, L8
Figueira, P., Santos, N. C., Pepe, F., Lovis, C., & Nardetto, N. 2013, A&A, 557, A93
Fischer, D. A. & Valenti, J. 2005, ApJ, 622, 1102

Flower, P. J. 1996, ApJ, 469, 355
Forveille, T., Bonfils, X., Delfosse, X., et al. 2009, A&A, 493, 645
Fuhrmann, K., Pfeiffer, M. J., & Bernkopf, J. 1998, A&A, 336, 942
Gastine, T., Yadav, R. K., Morin, J., Reiners, A., & Wicht, J. 2014, MNRAS, 438, L76
Gonzalez, G. 1998, A&A, 334, 221
Gregory, P. C. 2011, MNRAS, 415, 2523
Haywood, M. 2008, A&A, 482, 673
Huélamo, N., Figueira, P., Bonfils, X., et al. 2008, A&A, 489, L9
Ida, S. & Lin, D. N. C. 2004, ApJ, 616, 567
Ivanov, E. V. 2007, Advances in Space Research, 40, 959
Jenkins, J. S., Tuomi, M., Brasser, R., Ivanyuk, O., & Murgas, F. 2013, ApJ, 771, 41
Johnson, J. A., Aller, K. M., Howard, A. W., & Crepp, J. R. 2010, PASP, 122, 905
Kipping, D. M. 2013, MNRAS, 434, L51
Lanza, A. F., Rodonò, M., Pagano, I., Barge, P., & Llebaria, A. 2003, A&A, 403, 1135
Lovis, C., Dumusque, X., Santos, N. C., et al. 2011a, ArXiv e-prints
Lovis, C., Ségransan, D., Mayor, M., et al. 2011b, A&A, 528, A112
Mamajek, E. E. & Hillenbrand, L. A. 2008, ApJ, 687, 1264
Masana, E., Jordi, C., & Ribas, I. 2006, A&A, 450, 735
Mayor, M., Marmier, M., Lovis, C., et al. 2011, ArXiv e-prints
Mordasini, C., Alibert, Y., & Benz, W. 2009, A&A, 501, 1139
Mordasini, C., Alibert, Y., Benz, W., Klahr, H., & Henning, T. 2012, A&A, 541, A97
Mortier, A., Santos, N. C., Sousa, S., et al. 2013, A&A, 551, A112
Mortier, A., Santos, N. C., Sozzetti, A., et al. 2012, A&A, 543, A45
Naef, D., Mayor, M., Benz, W., et al. 2007, A&A, 470, 721
Nardetto, N., Mourard, D., Kervella, P., et al. 2006, A&A, 453, 309
Noyes, R. W., Hartmann, L. W., Baliunas, S. L., Duncan, D. K., & Vaughan, A. H. 1984, ApJ, 279, 763
Pepe, F., Lovis, C., Ségransan, D., et al. 2011, A&A, 534, A58
Pepe, F. A., Cristiani, S., Rebolo Lopez, R., et al. 2010, in SPIE Conference Series, Vol. 7735
Prato, L., Huerta, M., Johns-Krull, C. M., et al. 2008, ApJL, 687, L103
Queloz, D., Henry, G. W., Sivan, J. P., et al. 2001, A&A, 379, 279
Quirrenbach, A., Amado, P. J., Caballero, J. A., et al. 2014, in IAU Symposium, Vol. 299, IAU Symposium, ed. M. Booth, B. C. Matthews, & J. R. Graham, 395–396
Reid, I. N. 2002, PASP, 114, 306
Reiners, A. 2006, A&A, 446, 267
Reinhold, T., Reiners, A., & Basri, G. 2013, A&A, 560, A4
Saar, S. H. & Cuntz, M. 2001, MNRAS, 325, 55
Santos, N. C., Bouchy, F., Mayor, M., et al. 2004a, A&A, 426, L19
Santos, N. C., Gomes da Silva, J., Lovis, C., & Melo, C. 2010, A&A, 511, A54+
Santos, N. C., Israelian, G., & Mayor, M. 2001, A&A, 373, 1019
Santos, N. C., Israelian, G., & Mayor, M. 2004b, A&A, 415, 1153
Santos, N. C., Mayor, M., Bonfils, X., et al. 2011, A&A, 526, A112
Santos, N. C., Mayor, M., Bouchy, F., et al. 2007, A&A, 474, 647
Santos, N. C., Mayor, M., Naef, D., et al. 2002, A&A, 392, 215
Santos, N. C., Udry, S., Mayor, M., et al. 2003, A&A, 406, 373
Shkolnik, E., Walker, G. A. H., & Bohlender, D. A. 2003, ApJ, 597, 1092
Soubiran, C., Le Campion, J.-F., Cayrel de Strobel, G., & Caillo, A. 2010, A&A, 515, A111
Sousa, S. G., Santos, N. C., Israelian, G., et al. 2011a, A&A, 526, A99
Sousa, S. G., Santos, N. C., Israelian, G., Mayor, M., & Udry, S. 2011b, A&A, 533, A141+
Sousa, S. G., Santos, N. C., Mayor, M., et al. 2008, A&A, 487, 373
Sozzetti, A., Torres, G., Latham, D. W., et al. 2009, ApJ, 697, 544
Torres, G., Andersen, J., & Giménez, A. 2010, A&ARv, 18, 67
Tuomi, M. & Jones, H. R. A. 2012, A&A, 544, A116
Udry, S., Mayor, M., Benz, W., et al. 2006, A&A, 447, 361
Udry, S. & Santos, N. 2007, ARAA, 45, 397
van Leeuwen, F., ed. 2007, Astrophysics and Space Science Library, Vol. 350, Hipparcos, the New Reduction of the Raw Data
Vaughan, A. H. & Preston, G. W. 1980, PASP, 92, 385
Zechmeister, M. & Kürster, M. 2009, A&A, 496, 577

Appendix A: Line Profile Analysis Suite

In a recent paper, Figueira et al. (2013) analyzed a series of line profile indicators and discussed how these can help us pinpoint a RV signal created by stellar phenomena. These indicators and the associated statistical tests are now wrapped up in a simple code made available in the ExoEarths software webpage[14]. A living version of it can be accessed through a bitbucket repository[15].

The program is run simply by calling it using python (i.e. *python LineProf.py*), with all the information being provided by an ASCII configuration file. No programming experience is thus required; we note however that the program was written in a modular way, so that it can be used as a building block for complex data analysis software.

The program reads automatically a list of FITS files (e.g. HARPS-N or HARPS-S), or ASCII data with the CCFs to analyze. It applies the indicators presented in Figueira et al. (2013), and evaluates the correlation between such indicators and RVs. Then 100 000 non-correlated data sets are obtained by doing a Fisher-Yates shuffle of the data pairs, and the correlation of the original set compared with the correlation of the shuffled set. The z-value is provided, along with the (Gaussian) probability that the correlation is drawn from an uncorrelated data set. All these results are stored in ASCII files, and paper-quality plots for all the indicators selected are generated. The program can digest several dozens of files and do the complete analysis in a couple of minutes on a normal desktop/laptop.

[14] `http://www.astro.up.pt/exoearths/tools.html`
[15] `https://bitbucket.org/pedrofigueira/line-profile-indicators`